A two-tiered physiologically based model for dually labeled single-chain Fv-Fc antibody fragments

Gregory Z. Ferl,[1,2] Vania Kenanova,[2,3] Anna M. Wu,[2] and Joseph J. DiStefano III[1]

[1]Biocybernetics Laboratory, Departments of Computer Science and Medicine and Biomedical Engineering Interdepartmental Program, University of California, Los Angeles; [2]Department of Molecular and Medical Pharmacology, Crump Institute for Molecular Imaging, David Geffen School of Medicine at University of California at Los Angeles, Los Angeles; and [3]Division of Molecular Biology, Beckman Research Institute of the City of Hope, Duarte, California

Abstract

Monoclonal antibodies (mAb) are being used at an increasing rate in the treatment of cancer, with current efforts focused on developing engineered antibodies that exhibit optimal biodistribution profiles for imaging and/or radioimmunotherapy. We recently developed the single-chain Fv-Fc (scFv-Fc) mAb, which consists of a single-chain antibody Fv fragment (light-chain and heavy-chain variable domains) coupled to the IgG1 Fc region. Point mutations that attenuate binding affinity to FcRn were introduced into the Fc region of the wild-type scFv-Fc mAb, resulting in several new antibodies, each with a different half-life. Here, we describe the construction of a two-tiered physiologically based pharmacokinetic model capable of simulating the apparent biodistribution of both ^{111}In- and ^{125}I-labeled scFv-Fc mAbs, where ^{111}In-labeled metabolites from degraded ^{111}In-labeled mAbs tend to become trapped within the lysosomal compartment, whereas free ^{125}I from degraded ^{125}I-labeled mAbs is quickly eliminated via the urinary pathway. The different concentration-time profiles of ^{111}In- and ^{125}I-labeled mAbs permits estimation of the degradation capacity of each organ and elucidates the dependence of cumulative degradation in liver, muscle, and skin on FcRn affinity and tumor mass. Liver is estimated to account for ~50% of all degraded mAb when tumor is small (~0.1 g) and drops to about 35% when tumor mass is larger (~0.3 g). mAb degradation in residual carcass (primarily skin and muscle) decreases from ~45% to 16% as FcRn affinity of the three mAb variants under consideration increases. In addition, elimination of a small amount of mAb in the kidneys is shown to be required for a successful fit of model to data. [Mol Cancer Ther 2006;5(6):1550–8]

Received 2/7/06; revised 3/29/06; accepted 4/21/06.

Grant support: NIH Tumor Immunology Training grant 5-T32-CA009120-28, University of California at Los Angeles Graduate Division Dissertation Year Fellowship (G.Z. Ferl), Owen Witte and the Department of Microbiology, Immunology and Molecular Genetics (G.Z. Ferl) and NIH P01 CA43904 (V. Kenanova and A.M. Wu).

The costs of publication of this article were defrayed in part by the payment of page charges. This article must therefore be hereby marked advertisement in accordance with 18 U.S.C. Section 1734 solely to indicate this fact.

Requests for reprints: Gregory Z. Ferl, Department of Molecular and Medical Pharmacology, David Geffen School of Medicine at the University of California at Los Angeles, B2-085E CHS, 10833 Le Conte Avenue, Los Angeles, CA 90095-6948. Phone: 310-267-2495; Fax: 310-825-4517. E-mail: gferl@mednet.ucla.edu

doi:10.1158/1535-7163.MCT-06-0072

Introduction

Radioimmunotherapy and Engineered Monoclonal Antibodies

The use of radiolabeled monoclonal antibodies [mAb; Ibritumomab tiuxetan (Zevalin) and Tositumomab (Bexxar)] for the treatment of cancer (1, 2) necessitates the development of dosing schedules that minimize the exposure of healthy tissues to radiation while maximizing the radiation dose received by tumor. The goal of radioimmunotherapy is to deliver radiation in discrete amounts to tumor sites via a radionuclide that has been conjugated to an antitumor mAb. For example, Ibritumomab tiuxetan is an ^{90}Y-labeled mAb that binds specifically to CD20 (1, 2), a transmembrane protein expressed exclusively on both normal B cells and certain B cell–derived tumor cells, resulting in localization of mAb to tumor sites where ^{90}Y emits β-radiation capable of killing cells adjacent to the target cell (2). The benefit of this type of therapy is that tumor cells that do not express the target protein (e.g., CD20) can still be eliminated; however, exposure of healthy tissues to radiation is a major concern (3, 4). Effective tumor doses have been shown to be highly variable in clinical trials, ranging from 16 to 14,000 cGy, with toxicity reported following exposure of liver, stomach, bowel, kidneys, and lungs to doses ranging from 1,000 to 8,000 cGy, delivered by therapeutic doses of a variety of radionuclides (4). Bone marrow is especially sensitive to radiation, with toxicity reported following doses of 10 to 200 cGy (4).

Engineered antibodies have been developed in an effort to increase tumor targeting while reducing exposure of normal tissues. Most therapeutic mAbs are derived from immunoglobulin G (IgG, 150 kDa; ref. 5), which has a half-life of ~21 days in humans (6), resulting in excessive accumulation of radiolabeled mAbs in healthy tissues. The most common approach to this problem is reduction of mAb size via domain deletion (7), which decreases half-life and thereby reduces exposure of healthy tissues to radiation delivered by the mAb. Early efforts by Bird et al. produced the single-chain Fv (scFv) mAb fragment (8), a 26-kDa dimer composed of a light-chain variable region (V_L and J_L antigen-binding domains) and a heavy-chain variable region (V_H, D_H, and J_H antigen-binding domains) connected by a peptide linker. The scFv fragment exhibits rapid clearance and relatively low tumor uptake.

Subsequent efforts by other groups produced the scFv diabody (9, 10) and scFv-C_H3 minibody (11) in an effort to improve tumor uptake. The 55-kDa diabody is composed of two scFv fragments tethered together by a peptide linker and exhibits rapid blood clearance and higher tumor uptake compared with the scFv fragment. The 80-kDa minibody is composed of two separate scFv fragments joined to a C_H3 domain and shows superior tumor uptake and blood clearance when compared with the scFv and diabody.

Another method of controlling mAb half-life is through the introduction of amino acid substitutions into the Fc region (C_H2 and C_H3 constant domains) of the mAb. The neonatal Fc receptor (FcRn) has been shown to function as a protection receptor that increases IgG half-life via FcRn-IgG binding within the endosomal compartment of endothelial cells, diverting bound IgG away from the lysosomal degradation pathway and back into plasma (12, 13). Key residues that attenuate the binding affinity of IgG for FcRn have been identified within the IgG Fc domains (14), providing a mechanism for reducing mAb half-life without altering molecular weight.

Recently, we developed a 105-kDa scFv-Fc domain-deleted recombinant antibody fragment composed of an intact IgG1 Fc region bound to two scFv dimers (light-chain variable region-linker-heavy-chain variable region; ref. 15); half-life and tumor uptake of the wild-type (WT) scFv-Fc fragment are similar to that of intact IgG1. The biodistribution of the WT scFv-Fc and five variants (H435R, H435Q, H310A, I253A, and H310-H435Q) has been studied. The variants have decreasing half-lives in the following order: WT > H435Q > I253A > H310A > H310-H435Q, with the H310-H435Q variant exhibiting a clearance rate similar to a $F(ab')_2$ fragment.

Metabolism and Clearance of Antibodies

IgG catabolism seems to be widely distributed, having been shown to occur in liver, skin, muscle, spleen, intestine, and tumor. The liver and peripheral tissues (e.g., skin and muscle) have been shown to be major sites of IgG catabolism, each accounting for ~25% to 50% of antibody degradation (6, 16, 17), whereas the spleen (17, 18), intestine (18), and tumor sites (19) have been shown to be minor degradation sites. The degradation rate within the endothelial cells lining the microvasculature of skin and muscle, where FcRn has been shown to be present in high concentrations (20), may be a function of total IgG concentration (21); the degradation rate within liver also seems to be variable and has been shown to be dependent on the glycosylation status of IgG (18).

In our current study, cumulative organ-specific antibody degradation is estimated by comparing the apparent biodistributions of a mAb population labeled with ^{111}In and ^{125}I. ^{111}In is conjugated to the mAb via the linker molecule 1,4,7,10-tetraazacyclododecane-*N*,*N*′,*N*″,*N*‴-tetraacetic acid, which binds to lysine residues within proteins via active ester chemistry (22). Tsai et al. showed that [^{111}In]1,4,7,10-tetraazacyclododecane-*N*,*N*′,*N*″,*N*‴-tetraacetic acid-ε-amino-lysine is the metabolic end product resulting from ^{111}In-labeled IgG degradation, and that [^{111}In]1,4,7,10-tetraazacyclododecane-*N*,*N*′,*N*″,*N*‴-tetraacetic acid-ε-amino-lysine injected into nude mice is not sequestered within organ space and is quickly eliminated from the body (22). The same group also showed that ^{111}In-labeled Fab fragments are taken up and degraded primarily by the kidneys, with only a minor amount taken up by other organs (22). ^{125}I is quickly cleared from cells upon degradation of ^{125}I-labeled antibodies (23).

These data suggest a model where ^{125}I- and ^{111}In-labeled mAbs are taken up and degraded primarily in liver, skin, and muscle, where ^{111}In-labeled fragments are trapped within the lysosomal compartment and slowly cleared from cells, whereas free iodine is quickly cleared from cells and the body. Once cleared from cells, [^{111}In]1,4,7,10-tetraazacyclododecane-*N*,*N*′,*N*″,*N*‴-tetraacetic acid-ε-amino-lysine is quickly eliminated from the body, whereas larger fragments are taken up and degraded in the kidneys.

Physiologically Based Model of mAb Biodistribution

Based on our previous model of antibody biodistribution (24), we constructed a physiologically based model capable of describing the biodistribution of dually labeled mAb

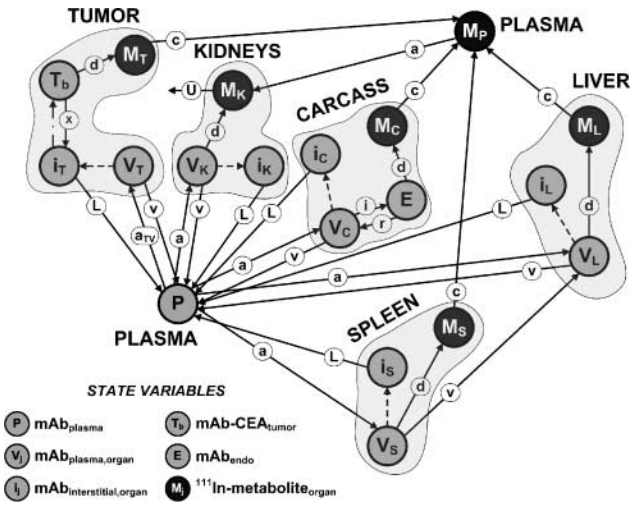

Figure 1. Compartmental representation of PBPK model. Model structure for fitting scFv-Fc biodistribution data collected from tumor-bearing and non–tumor-bearing mice. Each state variable is represented as a single compartment, connected to other compartments by arrows representing mass flux. State variables *P*, V_j, i_j, and *E* represent mAb in the central plasma pool, organ vascular space, organ interstitial space, and endothelial cell (intracellular) space, respectively; T_b, CEA-bound mAb; M_j, mAb metabolites. *j* = tumor (*T*), kidneys (*K*), carcass (*C*), liver (*L*), or spleen (*S*). Flux arrows labeled with a single letter represent linear, time-invariant mass transfer via arterial blood flow (*a*), venous blood flow (*v*), lymph flow (*L*), renal elimination (*U*), internalization by endothelial cells (*i*), recycling from endothelial cell to plasma (*r*), degradation within an organ (*d*), clearance of labeled metabolite from organ (*c*), or dissociation from CEA (*X*). The subscript TV indicates linear, time-varying mass transfer. Nonlinear mass fluxes include mass action based antibody binding to CEA (–·–·–). The dashed lines (– – –) represent antibody extravasation described by the two-pore macromolecule extravasation submodel (34). See Supplementary Material (available at http://mct.aacrjournals.org/) for model equations and fixed parameter values. See Table 1 for fitted parameter values.

Table 1. Optimized parameter estimates based on scFv-Fc biodistribution studies

Parameters	Units	DM_t*		DM_{nt}*		I253A†		WT†	
		Value × 10^{-4}	%CV	Value × 10^{-4}	%CV	Value × 10^{-4}	%CV	Value × 10^{-4}	%CV
$J_{iso,carcass,sp}$	mL·min^{-1} g^{-1}	1.45	16	DM_t	NA	1.59	19	I253A	NA
$J_{iso,kidney,sp}$	mL·min^{-1} g^{-1}	2.51	32	DM_t	NA	0.89	38	I253A	NA
$J_{iso,liver,sp}$	mL·min^{-1} g^{-1}	1.16	58	DM_t	NA	3.58	18	5.88	238
$J_{iso,spleen,sp}$	mL·min^{-1} g^{-1}	0.16	195	DM_t	NA	DM_t	NA	DM_t	NA
$J_{iso,tumor,sp}$	mL·min^{-1} g^{-1}	15.3	6.8	NA	NA	16.7	5	21.4	27
$k_{deg,FcRn}$	min^{-1}	52.8	63	27.4	41	52.2	165	I253A	NA
$k_{deg,kidney}$	mL·min^{-1}	0.80	33	2.8	7.1	1.27	15	DM_t	NA
$k_{deg,liver}$	mL·min^{-1}	15.6	5.8	17.6	7.8	4.02	8	2.71	234
$k_{deg,spleen}$	mL·min^{-1}	0.31	10	0.28	9.3	0.17	10	I253A	NA
$k_{deg,tumor}$	mL·min^{-1}	0.66	13	NA	NA	1.24	11	2.10	143
k_{int}	mL·min^{-1}	14.7	6.8	14.5	7.5	DM_t	NA	DM_t	NA
k_{M_P,M_C}	min^{-1}	1.02	39	0.60	46	1.57	38	I253A	NA
k_{M_P,M_L}	min^{-1}	2.77	10	2.05	18	4.06	16	I253A	NA
k_{M_P,M_S}	min^{-1}	0.67	59	0.76	50	1.79	30	I253A	NA
k_{M_P,M_T}	min^{-1}	5.25	40	NA	NA	5.58	47	I253A	NA
$k_{V_C,E}$	min^{-1}	0	NA	0	NA	121	165	867	752
$L_{carcass,sp}$	mL·min^{-1} g^{-1}	2.71	12	DM_t	NA	2.35	16	I253A	NA
$L_{kidney,sp}$	mL·min^{-1} g^{-1}	14.5	35	DM_t	NA	15.4	47	I253A	NA
$L_{liver,sp}$	mL·min^{-1} g^{-1}	11.3	56	DM_t	NA	10.9	23	21.1	260
$L_{spleen,sp}$	mL·min^{-1} g^{-1}	5.20	90	DM_t	NA	1.94	29	I253A	NA
$L_{tumor,sp}$	mL·min^{-1} g^{-1}	0	NA	NA	NA	0	NA	0.79	446
U	min^{-1}	92.8	10	34.0	12	67.5	8	I253A	NA

NOTE: Each parameter estimate is shown with the corresponding %CV. Parameter values that are shared between models are indicated by DM_t or I253A. Parameters are defined in the Supplementary Material (available at http://mct.aacrjournals.org/).
Abbreviation: NA, not available.
*DM_t and DM_{nt} were simultaneously fitted to all data shown in Fig. 2.
†I253A and WT were fitted separately to the data shown in Figs. 4 and 5.

fragments. Our new model uses kinetic information provided by several ^{111}In/^{125}I-labeled scFvFc variants, allowing us to quantify the degradative capacity of each organ and its relationship to FcRn affinity and tumor mass, which vary between mAb fragments and experimental animal groups, respectively.

From Mouse to Man

Translating modeling results from mouse to human is a challenging problem that is partially addressed by allometric scaling. Some physiologic, species-specific model parameters (e.g., volume flow rates) can be translated across species using the allometric equation, an empirical power law that relates the biological parameter to body weight (25, 26). Hence, the mathematical model can be parameterized using animal data and then ''scaled-up'' to human and used to predict the biodistribution of the same drug in the clinic (27). Other interspecies differences that can potentially affect drug pharmacokinetics, such as production and clearance rates of free antigen in blood and binding to target antigen in normal tissues, can be accounted for by making structural changes to the model when scaling from mouse to human.

Materials and Methods

Biological Data for Fitting the Models

Briefly, anti-carcinoembryonic antigen scFv-Fc cT84.66 mAbs labeled with ^{111}In, ^{125}I, or ^{131}I were injected into tumor-bearing female nude mice at $t = 0$. LS174T human colorectal tumor cells were flank injected into mice 10 days before ($t = -10$ days) administering radiolabeled antibody.[4] Tumor mass at $t = 0$ ranged from 0.003 to 0.229 g (median mass = 0.05 g, $n = 20$). Mice in each of four experimental groups ($n = 5$) were sacrificed at the following timed data points: 0, 2, 4, 6, 12, 24, 48, and 72 hours. Liver, lungs, spleen, kidneys, and tumor were excised, weighed, and counted for remaining radioactivity. Biodistribution profiles were created for the WT scFv-Fc mAb along with three variants containing the following amino acid substitutions: H310A-H435Q (henceforth referred to as double mutant), H310A, and I253A. ^{111}In- and ^{125}I-labeled double mutant mAbs were coinjected into the same mice as were ^{111}In- and ^{125}I-labeled I253A mAbs; ^{125}I-labeled WT mAbs were coinjected with ^{131}I-labeled I253A mAbs. An additional study was done, in which ^{111}In- and ^{125}I-labeled double mutant mAbs were coinjected into non–tumor-bearing nude mice. The H310A data set was not used in model development because there is no statistically significant difference ($P > 0.1$, two-way ANOVA) between the H310A and double mutant plasma curves, as calculated using GraphPad Prism.[5]

[4] V. Kenanova et al., unpublished data.
[5] GraphPad Prism 4.03. Windows ed: GraphPad Software, San Diego, CA (http://www.graphpad.com).

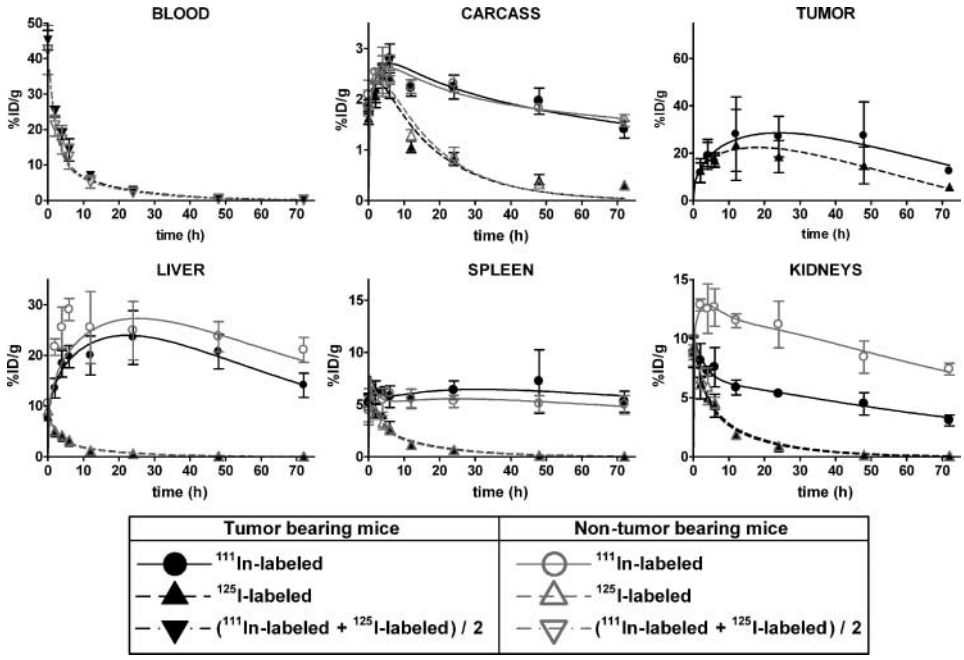

Figure 2. PBPK model fitted to double mutant biodistribution data. The two PBPK models (DM_t and DM_{nt}) were simultaneously fitted to all data sets (Table 1), shown by the set of black and gray curves. *Open circles* and *triangles,* apparent biodistribution of ^{111}In- and ^{125}I-labeled double mutant mAbs, respectively, in non–tumor-bearing mice; *closed shapes,* data taken from tumor-bearing mice. *Points,* mean of 5 mice; *bars,* SD. Because there was no statistically significant difference ($P > 0.1$, two-way ANOVA)[5] between the ^{111}In and ^{125}I concentration-time profiles in plasma, the mean of these values was used (*inverted triangle*). *Points,* mean of 10 mice; *bars,* SD.

Mathematical Model Development

Here, we use a modified version of the physiologically based pharmacokinetic (PBPK) model presented in Ferl et al. (24). Tumor, kidneys, residual carcass, liver, and spleen are explicitly represented along with the central plasma pool (Fig. 1). Degradation terms, flux d in Fig. 1, connect the intact scFv-Fc submodel (light gray compartments in Fig. 1) to the ^{111}In-labeled mAb fragment submodel (dark gray compartments) and are included in tumor, kidneys, carcass, liver, and spleen. Tumor and all organ pools contain compartments representing interstitial (state variable i_j in Fig. 1) and vascular (V_j) spaces; tumor has an additional compartment for carcinoembryonic antigen–bound mAb (T_b). Compartment M_j represents ^{111}In-labeled metabolites trapped within organ j for a length of time determined by the linear efflux rate, flux c. ^{111}In-labeled fragments that are released from the organ pool reenter the central plasma compartment (M_P). ^{111}In-labeled mAb fragments are transported from M_P to the kidneys via the arterial circulation, where they are trapped for a period of time determined by the linear excretion rate, flux U. All FcRn-mAb interactions take place within a single compartment (E), shown in the residual carcass pool. Antibody is internalized via nonspecific bulk fluid uptake (flux i) into endothelial cells (E), where unbound antibody is degraded (flux d), and FcRn-bound antibody is recycled back into plasma (flux r). Free and FcRn bound antibody are both represented by compartment E, allowing FcRn-mAb interactions to be described without explicitly including parameters that have not been directly measured *in vivo* (FcRn concentration, on-off rates for FcRn-mAb interaction). See Supplementary Material for model equations and parameter values.[6]

Data Fitting and Parameter Estimation

The PBPK model shown in Fig. 1 was fitted to data for each scFv-Fc variant (double mutant, I253A, and WT) using the kinetic modeling program SAAM II (28). Parameter values for our new model were obtained as follows: 24 parameter values were taken from the literature (29–32); 5 were measured experimentally; and the remaining 22 (Table 1) were fitted to the data using an extended least-squares objective function (33) and the relative data weighting scheme (34) provided by SAAM II. Identifiability of these 22 model parameters was established numerically during preliminary data fitting procedures, evidenced by the reasonable parameter estimate variances in Table 1.

As shown in Table 1, each of the four models share certain parameter values; that is, although there are 22 unknown parameters across all models, each individual model (double mutant, I253A, and WT) contains <22 unknown parameters, as described below.

Double Mutant Tumor-Bearing and Double Mutant Non–Tumor-Bearing Models (20 Unknown Parameters). First, we simultaneously estimated unknown parameters for the double mutant tumor-bearing (DM_t) and double mutant non–tumor-bearing (DM_{nt}) models. The double mutant variant has a plasma concentration-time profile (Fig. 2) approximately equal to that of the $F(ab')_2$ fragment (data not shown), which cannot bind FcRn due to the absence of an Fc region and clears from the body relatively quickly. This suggests that, as is the case with the $F(ab')_2$ fragment, the double mutant scFv-Fc fragment cannot be

[6] Supplementary material for this article is available at Molecular Cancer Therapeutics Online (http://mct.aacrjournals.org/).

recycled to plasma via FcRn binding or that binding occurs with very low affinity, resulting in a negligible level of mAb recycling. Hence, the recycling rate for FcRn-bound mAb (flux r in Fig. 1) was set to 0 in the DM_t and DM_{nt} models. Flux L in the tumor pool was set to 0 in both double mutant models to improve numerical identifiability of model parameters and is justifiable because a functioning lymphatic system is typically not present within intratumor regions (35).

The biodistribution of double mutant scFv-Fc in tumor-bearing and non–tumor-bearing mice is similar, with the notable exception of ^{111}In-labeled mAb in kidneys (Fig. 2). To account for this difference, parameters within the ^{111}In-labeled mAb fragment submodel (fluxes d, c, U, and i) were allowed to vary between models during the fitting process; all other parameters were fixed between the two models (Table 1).

I253A Model (19 Unknown Parameters). Next, we estimated unknown parameters for the I253A model. Flux i and parameter $J_{iso,spleen,sp}$ (see two-pore model in Supplementary Material, Eqs. 33–42)[6] were shown to be numerically unidentifiable; estimates provided by the $DM_{tumor\ bearing}$ model were used instead. L_{tumor} was also set to 0, as described earlier.

WT Model (7 Unknown Parameters). Lastly, we estimated unknown parameters for the WT model. Because no ^{111}In-labeled WT scFv-Fc data were collected, a number of parameters were unidentifiable and had to be fixed when fitting the PBPK model to the WT data set: $J_{iso,spleen,sp}$, k_{int}, and $k_{deg,kidney}$ were set to estimates provided by the DM_t model, whereas $J_{iso,liver,sp}$, $J_{iso,tumor,sp}$, $k_{deg,liver}$, $k_{deg,tumor}$, $k_{Vc,E}$, $L_{liver,sp}$, and $L_{tumor,sp}$ were fitted to the data. The remaining 12 parameters were set to estimates provided by the I253A model (Table 1). See Supplementary Material for parameter definitions.[6]

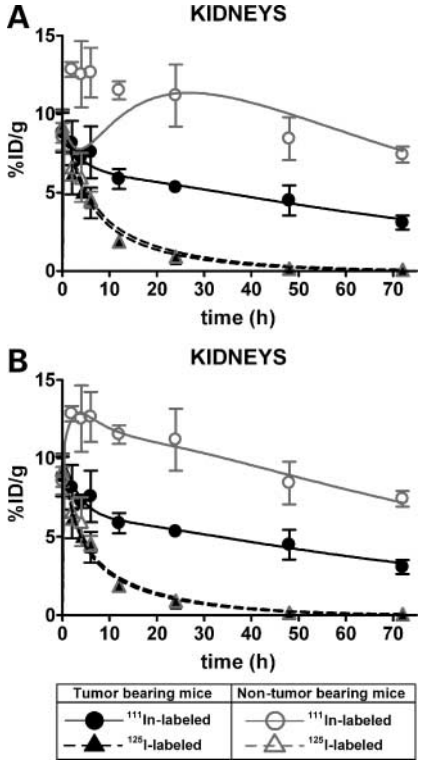

Figure 3. Addition of a degradation term to the kidneys pool of the double mutant model. **A,** fit to kidney data obtained when $k_{deg,kidney}$ (flux d in kidneys pool) is removed from the model structure shown in Fig. 1. **B,** improved fit obtained when the degradation term is added to the kidneys pool.

Variable Tumor Mass Submodel

The variable tumor mass submodel was used to describe tumor growth, including growth of a necrotic core, as described in Ferl et al. (24). Comparing the Gompertz equation (36) to linear regression, growth of total tumor mass over the course of the experiment was best described by the Gompertz equation for the I253A tumor growth data ($R^2_{Gompertz}$=0.96 and R^2_{linear}=0.89; data not shown). WT and double mutant tumor growth data are adequately described, qualitatively, by a straight line (data not shown). All tumor growth fits were done using GraphPad Prism.[5] For the WT model, perfusable tumor mass is set equal to total tumor mass because total mass does not exceed 0.1 g over the course of the experiment. Total tumor antigen concentration $B_{max,sp}$ was calculated as described in Ferl et al. (24).

Estimation of Cumulative Organ-Specific Degradation

Cumulative organ specific degradation was estimated by removing compartment M_P and all associated fluxes (i.e., parameters k_{M_P,M_L}, k_{M_P,M_S}, k_{M_P,M_C}, k_{M_P,M_T}, and k_{M_K,M_P} set to 0) from the PBPK model, so that degraded mAb collects in a single compartment, and implementing the following equation for each organ:

$$\mathrm{Deg}_j(t) = M_j(t)/\left[M_T(t_f) + M_K(t_f) + M_C(t_f) + M_L(t_f) + M_S(t_f)\right] \times 100\% \quad \text{(A)}$$

where t_f = 72 hours, $M_j(t)$ equals the amount of degraded mAb in the organ of interest at time t and j = T, K, C, L, or S. The denominator normalizes the curve so that $\mathrm{Deg}_j(t_f)$ is equal to the percentage of total degraded antibody that was degraded by the organ of interest over the course of the experiment.

Results

PBPK Model Fitted to DM_t and DM_{nt} Biodistribution Data

The curves shown in Fig. 2 represent PBPK model outputs for tumor-bearing and non–tumor-bearing mice fitted simultaneously to all double mutant biodistribution data (*circles* and *triangles*). ^{111}In and ^{125}I blood measurements were not statistically different ($P > 0.1$, two-way ANOVA)[5] and were averaged (*open* and *closed inverted triangles*). Parameter estimates and percent coefficients of variation (%CV) are listed in Table 1 (%CV range, 6–195%, with median %CV = 18%). As described in Materials and

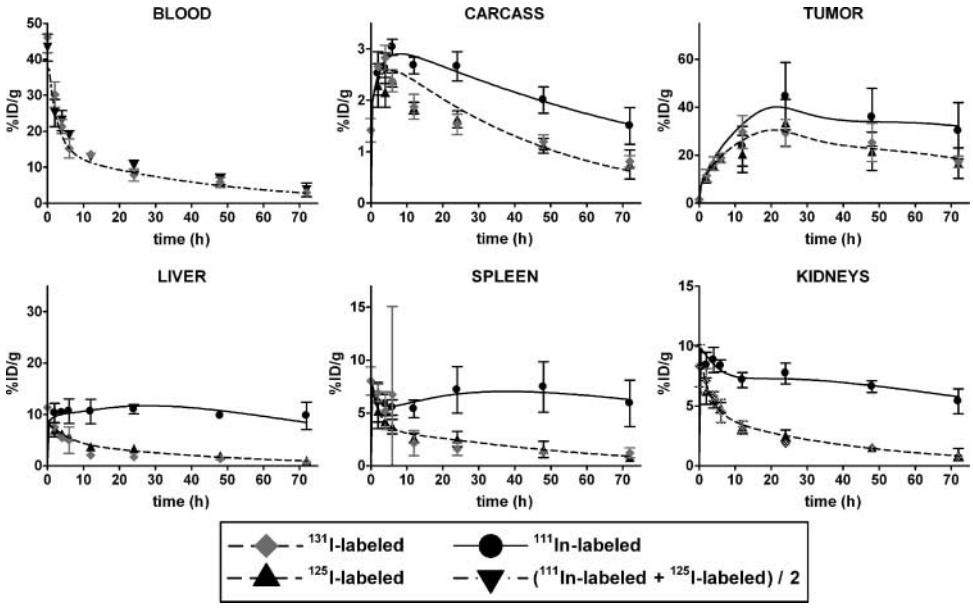

Figure 4. PBPK model fitted to I253A biodistribution data. Unknown model parameters were simultaneously fitted (*gray* and *black curves*) to three sets of biodistribution data from tumor-bearing mice (Table 1). *Solid circles, open circles*, and *open triangles,* apparent biodistribution of ^{111}In-, ^{125}I-, and ^{131}I-labeled I253A mAbs, respectively. *Points,* mean of 5 mice; *bars,* SD. Because there was no statistically significant difference ($P > 0.1$, two-way ANOVA[5] between the ^{111}In and ^{125}I concentration-time profiles in plasma, the mean of these values was used (*inverted triangle*). *Points,* mean of 10 mice; *bars,* SD.

Methods, parameters that characterize the ^{111}In-labeled mAb fragment submodel (dark gray compartments, Fig. 1) were independently varied within the DM_t and DM_{nt} models during the fitting process, as shown in Table 1, to account for the difference between the ^{111}In data points (*open* versus *closed circles*) in the kidney panel, as well as less pronounced differences in other organs. Table 1 shows that all of the aforementioned parameters have <2-fold difference in value between the two models (DM_t and DM_{nt}), with the exception of renal clearance (flux U), estimated to be ~2.7 times greater in tumor-bearing versus non–tumor-bearing mice and renal degradation (flux d in kidneys pool), estimated to be ~3.5 times greater in non–tumor-bearing versus tumor-bearing mice.

Degradation Term in the Kidneys Is Required to Fit Double Mutant Data

Because the amount of intact antibody degraded in the kidneys is unknown (previous estimates range, 0–15%; refs. 6, 17), we fitted the PBPK model describing scFv-Fc biodistribution to the DM_t and DM_{nt} data sets with and without a degradation term in the kidney pool (Fig. 3). Figure 3A shows that the model fit to the first 12 hours of data is qualitatively poor but can be improved by adding a degradation term to the kidneys pool, as shown in Fig. 1. The Akaike information criterion (AIC; ref. 37), a metric used for model discrimination, was calculated over plasma, tumor and all organ data fits by SAAM II (28) for the model lacking the kidneys leak ($AIC_{Fig.\ 3A} = 1.17$) and for the model with the kidney leak ($AIC_{Fig.\ 3B} = 1.05$). A lower AIC value indicates a better overall fit of model to data. All model parameters were fitted as described in Materials and Methods.

PBPK Model Fitted to I253A Biodistribution Data

As described in Materials and Methods, K_{int} and $J_{iso,spleen,sp}$ were fixed to the values estimated using the DM_t model ($K_{int} = 14.7 \times 10^{-4}$ mL min^{-1}, $J_{iso,spleen,sp} = 1.6 \times 10^{-5}$ mL min^{-1} g^{-1}). The solid and dashed curves in Fig. 4 represent the I253A PBPK model simultaneously fitted to all I253A data (*circles, diamonds*, and *triangles*). %CVs range from 5% to 165% with median %CV at 19%. ^{111}In and ^{125}I measurements taken in blood were not statistically different ($P > 0.1$, two-way ANOVA)[5] and were averaged (*closed inverted triangles*).

PBPK Model Fitted to WT Biodistribution Data

As described in Materials and Methods, 15 of 22 unknown parameters for the WT model were fixed to values estimated using the DM_t and I253A models (Table 1). The remaining parameters were fitted to the WT data set. The dashed line in Fig. 5 represents the PBPK model (Fig. 1) fitted to WT ^{125}I data, and the solid line represents a *prediction* of ^{111}In biodistribution because no ^{111}In data was collected. %CVs range from 27% to 752%, with median %CV at 238%.

Comparison of All Model Parameter Estimates

Comparing the I253A and double mutant models, most estimated parameters have similar values (i.e., no more than a 2-fold difference between the models). $J_{iso,kidney,sp}$, $J_{iso,liver,sp}$, $J_{iso,spleen,sp}$, U, $k_{M_P M_S}$ and $k_{M_P M_C}$ all had ~2- to 3-fold differences between the two models, whereas $k_{deg,kidney}$ and $k_{deg,liver}$ had 3.5- and 4.4-fold differences, respectively. All estimated parameters for the WT model had values similar to those estimated for the I253A model (no more than 2-fold difference between models), with the exception of the recycling rate of FcRn-bound mAb back into plasma ($k_{Vc,E}$), which is ~7 times greater in the WT model ($k^{I253A}_{Vc,E} = 0.012$ min^{-1}, $k^{WT}_{Vc,E} = 0.087$ min^{-1}). See Table 1 for fitted parameter values.

Estimation of Cumulative Organ-Specific Degradation

Estimates of cumulative organ-specific degradation over the course of each experiment are shown in Fig. 6, where each data point on the top portion of the graph is calculated

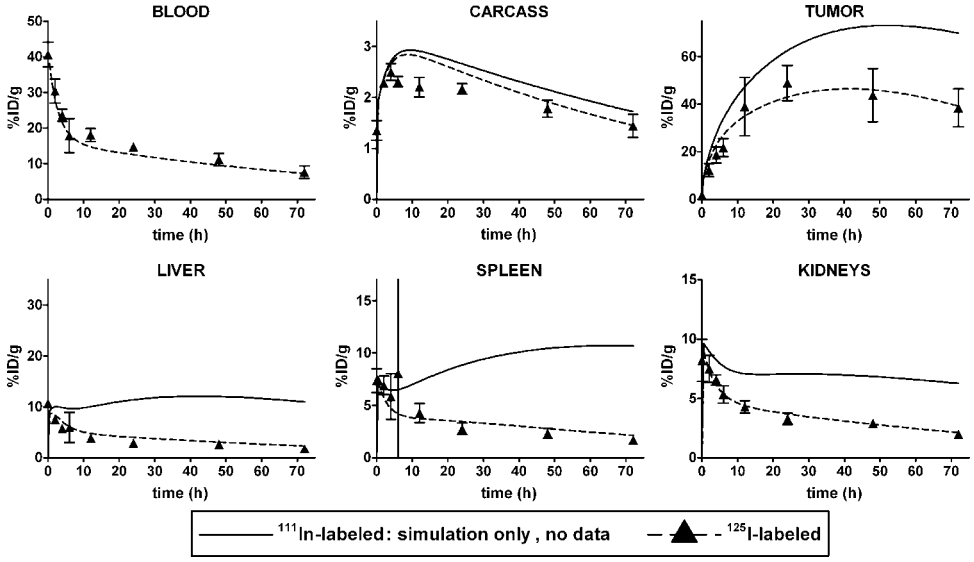

Figure 5. PBPK model fitted to WT biodistribution data. Unknown model parameters were fitted to a single set of biodistribution data from tumor-bearing mice (Table 1). *Triangles,* apparent biodistribution of ^{125}I-labeled WT mAbs. *Points,* mean of 5 mice; *bars,* SD. *Dotted lines,* PBPK model fitted to biodistribution data; *solid lines,* prediction of ^{111}In-labeled WT mAb biodistribution.

using Eq. A at $t = t_f = 72$ hours, when all Deg_j values are essentially constant. At the end of each experiment, cumulative degradation in liver was 48%, 35%, and 52% of total degraded double mutant, I253A, and WT mAb in tumor-bearing mice, respectively; residual carcass has degraded 45%, 39%, and 16%, respectively; tumor has degraded 4%, 13%, and 13%, respectively; kidneys has degraded 3%, 11%, and 16%, respectively; and the spleen has degraded 1%, 1%, and 3%, respectively. Cumulative degradation amounts are also shown for non–tumor-bearing mice, where liver, carcass, kidneys, and spleen account for 50%, 41%, 8%, and 1% of total degraded double mutant mAb, respectively. Tumor mass is shown on the bottom portion of the graph.

Discussion

Our model suggests that mAb kinetics depend on tumor size and mAb binding affinity for FcRn, which decreases in the order WT > I253A > double mutant. As expected, the estimated amount of mAb degraded in carcass increases from 16% in the WT experiments to 39% and 45% in the I253A and double mutant experiments (Fig. 6), respectively, further validating the putative mechanism for the protective role of FcRn in IgG catabolism. However, mAb degradation in liver shows a pattern that is not as strongly dependent on FcRn affinity, with ~48% to 52% of mAb degraded in the WT and double mutant experiments, and only about 35% degraded in the I253A experiments (Fig. 6). The lower cumulative degradation may be due to an approximate doubling of tumor mass in the I253A experiments (0.301 g) compared with the double mutant (0.156 g) and WT (0.107 g) experiments (Fig. 6). The larger tumor, present only in the I253A studies, draws a significant amount of mAb, possibly changing the kinetics so that less mAb is degraded in liver. Evidence that the presence of tumor, independent of FcRn affinity, can alter mAb kinetics in other organs can be seen when comparing double mutant biodistributions in normal and tumor-bearing mice. Figure 2 shows that the concentration of ^{111}In-labeled double mutant mAb fragment is significantly higher ($P > 0.1$, two-way ANOVA)[5] in liver and kidneys in non–tumor-bearing versus tumor-bearing mice.

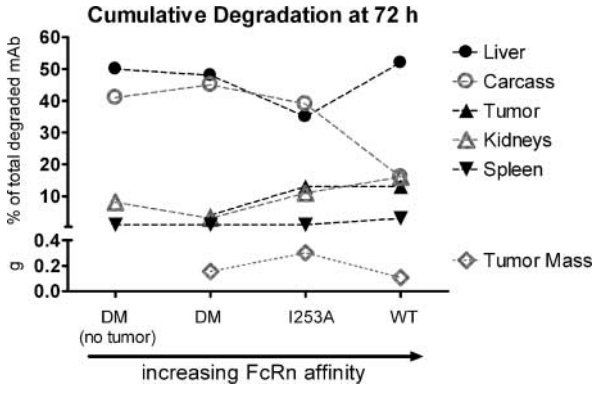

Figure 6. Estimated organ-specific degradation. Cumulative amounts of mAb degradation that occurs in liver, carcass, tumor, kidneys, and spleen as percentage of total amount of antibody degraded at 72 h. *Bottom,* tumor mass in grams.

Addition of a mAb degradation term to the kidneys pool improves the fit to data from non–tumor-bearing mice (Fig. 3), suggesting that a small amount of scFv-Fc is degraded in the kidneys. We estimate that across all experimental mouse groups, 3% to 16% of total degraded scFv-Fc is taken up and catabolized within the kidneys by the end of the study. This is in agreement with published estimates of 0% to 15% for intact mAb (150 kDa) degradation in kidneys (6, 17). The degradation term could also be interpreted as loss of ^{111}In label from mAb within the kidneys in addition to metabolic degradation. Model fits to other organ data are not adversely affected by the presence of a degradation term in the kidneys,

shown by comparison of AIC values calculated over plasma, tumor, and all organ data fits ($AIC_{Fig.\ 3B}$ =1.05, $AIC_{Fig.\ 3A}$ =1.17). The spleen played a minor role in antibody degradation in all cases, eliminating no more than 3% of all degraded scFv-Fc. Interestingly, estimated cumulative degradation for each scFv-Fc variant (WT, I253A, and double mutant) in kidneys seems to parallel degradation in tumor; kidneys and tumor account for 3% to 4% of estimated scFv-Fc degradation in the double mutant experiments and 11% to 13% and 13% to 16% in the I253A and WT experiments, respectively. It is unclear how the metabolic activity of tumor may affect uptake and degradation of scFv-Fc in kidneys.

Radiolabeled mAbs are increasingly being used for the treatment of cancer. Application of mathematical models to the problem of antibody design and optimal dosing (i.e., regimens that maximize drug concentration within tumor while minimizing drug distribution to healthy tissues) holds potential for increasing overall drug efficacy. Physiologically based models that describe concentration-time profiles on a per organ basis can be used to meet this goal but often contain a large number of unknown parameters that must be estimated by fitting the model to data. We have shown here that dually labeled mAb kinetic studies provide the needed data for complete quantification of a two-tiered PBPK model that describes kinetics of intact mAb and its metabolites, providing a more detailed picture of the interaction between drug and organs. A major result of these studies is that the biodistributions of ^{111}In- and ^{125}I-labeled mAbs, measured experimentally, was used to estimate cumulative degradation within each organ and its dependence on FcRn affinity and tumor mass, allowing us to move well beyond the representation of mAb elimination as a single leak from the kidneys or plasma, as has been done in previous models (29, 38, 39). Additionally, scFv-Fc degradation and/or loss of label from mAb in the kidneys were shown to be significant. Our two-tiered PBPK model allows us to extract additional information from ^{111}In- and ^{125}I-labeled mAb biodistribution data, providing insight into mAb kinetics and creating a tool that can potentially be used to assist in the design of antibody-based therapeutics and optimal dosing schedules in the clinic.

Acknowledgments

We thank Owen Witte and Sharon Hori for their helpful advice.

References

1. Sharkey RM, Goldenberg DM. Perspectives on cancer therapy with radiolabeled monoclonal antibodies. J Nucl Med 2005;46 Suppl 1:115 – 27S.

2. Harris M. Monoclonal antibodies as therapeutic agents for cancer. Lancet Oncol 2004;5:292 – 302.

3. Wu AM, Senter PD. Arming antibodies: prospects and challenges for immunoconjugates. Nat Biotechnol 2005;23:1137 – 46.

4. Meredith R. Clinical trial design and scoring of radionuclide therapy endpoints: normal organ toxicity and tumor response. Cancer Biother Radiopharm 2002;17:83 – 99.

5. Carter P. Improving the efficacy of antibody-based cancer therapies. Nat Rev Cancer 2001;1:118 – 29.

6. Waldmann TA, Strober W. Metabolism of immunoglobulins. Prog Allergy 1969;13:1 – 110.

7. Wu AM, Yazaki PJ. Designer genes: recombinant antibody fragments for biological imaging. Q J Nucl Med 2000;44:268 – 83.

8. Bird RE, Hardman KD, Jacobson JW, et al. Single-chain antigen-binding proteins. Science 1988;242:423 – 6.

9. Mallender WD, Voss EW, Jr. Construction, expression, and activity of a bivalent bispecific single-chain antibody. J Biol Chem 1994;269: 199 – 206.

10. Holliger P, Prospero T, Winter G. ''Diabodies'': small bivalent and bispecific antibody fragments. Proc Natl Acad Sci U S A 1993;90: 6444 – 8.

11. Hu S, Shively L, Raubitschek A, et al. Minibody: a novel engineered anti-carcinoembryonic antigen antibody fragment (single-chain Fv-CH3) which exhibits rapid, high-level targeting of xenografts. Cancer Res 1996; 56:3055 – 61.

12. Ghetie V, Ward ES. Transcytosis and catabolism of antibody. Immunol Res 2002;25:97 – 113.

13. Simister NE. Placental transport of immunoglobulin G. Vaccine 2003; 21:3365 – 9.

14. Kim JK, Firan M, Radu CG, Kim CH, Ghetie V, Ward ES. Mapping the site on human IgG for binding of the MHC class I-related receptor, FcRn. Eur J Immunol 1999;29:2819 – 25.

15. Kenanova V, Olafsen T, Crow DM, et al. Tailoring the pharmacokinetics and positron emission tomography imaging properties of anti-carcinoembryonic antigen single-chain Fv-Fc antibody fragments. Cancer Res 2005;65:622 – 31.

16. Fukumoto T, Brandon MR. Importance of the liver in immunoglobulin catabolism. Res Vet Sci 1982;32:62 – 9.

17. Henderson LA, Baynes JW, Thorpe SR. Identification of the sites of IgG catabolism in the rat. Arch Biochem Biophys 1982;215:1 – 11.

18. Wright A, Sato Y, Okada T, Chang K, Endo T, Morrison S. *In vivo* trafficking and catabolism of IgG1 antibodies with Fc associated carbohydrates of differing structure. Glycobiology 2000;10: 1347 – 55.

19. Rogers BE, Franano FN, Duncan JR, et al. Identification of metabolites of ^{111}In-diethylenetriaminepentaacetic acid-monoclonal antibodies and antibody fragments *in vivo*. Cancer Res 1995;55:5714 – 20s.

20. Borvak J, Richardson J, Medesan C, et al. Functional expression of the MHC class I-related receptor, FcRn, in endothelial cells of mice. Int Immunol 1998;10:1289 – 98.

21. Brambell FW, Hemmings WA, Morris IG. A theoretical model of gamma-globulin catabolism. Nature 1964;203:1352 – 4.

22. Tsai SW, Li L, Williams LE, Anderson AL, Raubitschek AA, Shively JE. Metabolism and renal clearance of ^{111}In-labeled DOTA-conjugated antibody fragments. Bioconjug Chem 2001;12:264 – 70.

23. Koizumi M, Endo K, Watanabe Y, et al. Pharmacokinetics of internally labeled monoclonal antibodies as a gold standard: comparison of biodistribution of ^{75}Se-, ^{111}In-, and ^{125}I-labeled monoclonal antibodies in osteogenic sarcoma xenografts in nude mice. Cancer Res 1989;49: 1752 – 7.

24. Ferl GZ, Wu AM, Distefano JJ III. A predictive model of therapeutic monoclonal antibody dynamics and regulation by the neonatal Fc receptor (FcRn). Ann Biomed Eng 2005;33:1640 – 52.

25. Dedrick RL. Animal scale-up. J Pharmacokinet Biopharm 1973;1: 435 – 61.

26. Hu TM, Hayton WL. Allometric scaling of xenobiotic clearance: uncertainty versus universality. AAPS PharmSci 2001;3:E29.

27. Baxter LT, Zhu H, Mackensen DG, Butler WF, Jain RK. Biodistribution of monoclonal antibodies: scale-up from mouse to human using a physiologically based pharmacokinetic model. Cancer Res 1995;55: 4611 – 22.

28. Barrett PH, Bell BM, Cobelli C, et al. SAAM II: simulation, analysis, and modeling software for tracer and pharmacokinetic studies. Metabolism 1998;47:484 – 92.

29. Baxter LT, Zhu H, Mackensen DG, Jain RK. Physiologically based pharmacokinetic model for specific and nonspecific monoclonal antibodies and fragments in normal tissues and human tumor xenografts in nude mice. Cancer Res 1994;54:1517 – 28.

30. Brown RP, Delp MD, Lindstedt SL, Rhomberg LR, Beliles RP.

Physiological parameter values for physiologically based pharmacokinetic models. Toxicol Ind Health 1997;13:407 – 84.

31. Hefta LJ, Neumaier M, Shively JE. Kinetic and affinity constants of epitope specific anti-carcinoembryonic antigen (CEA) monoclonal antibodies for CEA and engineered CEA domain constructs. Immunotechnology 1998;4:49 – 57.

32. Rippe B, Haraldsson B. Transport of macromolecules across microvascular walls: the two-pore theory. Physiol Rev 1994;74:163 – 219.

33. Heatherington AC, Vicini P, Golde H. A pharmacokinetic/pharmacodynamic comparison of SAAM II and PC/WinNonlin modeling software. J Pharm Sci 1998;87:1255 – 63.

34. Bell BM, Burke JV, Schumitzky A. A relative weighting method for estimating parameters and variances in multiple data sets. Comput Stat Data An 1996;22:119 – 35.

35. Padera TP, Stoll BR, Tooredman JB, Capen D, di Tomaso E, Jain RK. Pathology: cancer cells compress intratumour vessels. Nature 2004; 427:695.

36. Rygaard K, Spang-Thomsen M. Quantitation and Gompertzian analysis of tumor growth. Breast Cancer Res Treat 1997;46:303 – 12.

37. Akaike H. A new look at the statistical model identification. IEEE Trans Autom Control 1974;AC-19:716 – 23.

38. Covell DG, Barbet J, Holton OD, Black CD, Parker RJ, Weinstein JN. Pharmacokinetics of monoclonal immunoglobulin G1, F(ab′)2, and Fab′ in mice. Cancer Res 1986;46:3969 – 78.

39. Hansen RJ, Balthasar JP. Pharmacokinetic/pharmacodynamic modeling of the effects of intravenous immunoglobulin on the disposition of antiplatelet antibodies in a rat model of immune thrombocytopenia. J Pharm Sci 2003;92:1206 – 15.